Available online at www.sciencedirect.com
SCIENCE DIRECT®
International Journal of Heat and Mass Transfer 47 (2004) 3565–3572
International Journal of HEAT and MASS TRANSFER
www.elsevier.com/locate/ijhmt

Experimental data and model for heat transfer, in liquid falling film flow on shell-side, for spiral-wound LNG heat exchanger

Bengt O. Neeraas [a,*], Arne O. Fredheim [a], Bjørn Aunan [b]

[a] Statoil Research Center, 7005 Trondheim, Norway
[b] PGS Production AS, 7405 Trondheim, Norway

Received 15 February 2002; received in revised form 4 December 2003
Available online 19 March 2004

Abstract

A test plant has been constructed for measurements of local heat-transfer coefficients and frictional pressure drops on the shell-side of spiral-wound LNG heat exchangers.

Measurements have been performed with single-phase vapor flow, liquid film flow and two-phase shear flow. This paper focuses on the measurements and the results from the liquid falling film flow experiments.

One hundred and seventy-one liquid falling film heat-transfer measurements have been performed at a film *Re*-number range of 500–8000 with ethane, propane, methane/ethane mixture, ethane/propane mixtures and ethane/*n*-butane mixture as test fluids.

Keywords: Experimental; Film; Heat transfer; LNG

1. Introduction

The most important heat-transfer equipment in base-load LNG plants is the main cryogenic heat exchanger for cooling, condensation and liquefaction of the natural gas. The multi-stream spiral-wound type is the most commonly used heat exchanger for this application. Information regarding heat transfer and pressure drop models for spiral-wound heat exchangers is proprietary information for the very few manufacturers of such units. To be able to perform design and rating calculations and steady-state and dynamic process simulation of this type of equipment, reliable methods for calculation of heat-transfer coefficients and pressure drops are needed. In a spiral-wound heat exchanger used for LNG production the refrigerant evaporates on the shell-side in downward flow. The streams on the tube-side are condensing or single-phase natural gas and refrigerant. Two different test plants have been constructed for the purpose of measuring heat-transfer coefficients and pressure drop, both for shell-side evaporation and tube-side condensation. Based on the measurements models have been selected or developed.

A principle sketch of a multi-stream spiral-wound heat exchanger is depicted in Fig. 1 [1].

The different tubes are coiled in layers around the central core. The coiling direction alternates from one layer to the next. Radial and longitudinal distances between the tubes are held constant by use of space bars. The tubes are connected to tube sheets at both ends of the heat exchanger.

The Norwegian University of Science and Technology (NTNU) and SINTEF Energy Research have since 1984 worked with thermal design and laboratory measurements of heat-transfer coefficients and pressure drop

* Corresponding author. Address: Statoil Research Center, 7005 Trondheim, Norway. Fax: +47-73-58-43-45.
E-mail addresses: bone@statoil.com (B.O. Neeraas), aof@statoil.com (A.O. Fredheim), bjorn.aunan@pgs.com (B. Aunan).

0017-9310/$ - see front matter © 2004 Elsevier Ltd. All rights reserved.
doi:10.1016/j.ijheatmasstransfer.2004.01.009

Nomenclature

a	constant
a_1	constant
A	area (m^2)
b	constant
B_R	estimated uncertainty from systematic error
c	constant
c_p	isobaric specific heat capacity (J/kg K)
d	constant
D	diameter (m)
DP	differential pressure (Pa)
E	electric potential (mV)
g	gravity constant (m/s^2)
$\dot{m}$	flow rate (kg/s)
M	mass flux (kg/m^2 s)
N_{lay}	number of tube layers
Nu	Nusselt number
P	pressure (bar)
P_r	radial pitch between tube centers (m)
Pr	Prandtl number
R	resistance (Ω)
Re_l	film Reynolds number $= 4 \cdot \Gamma/\mu_l$
S_R	standard deviation from random errors
S_{in}	in-line radial distance between tube layers (m)
S_{ref}	radial distance between tube layers (m)
Q_{sec}	el.power supplied to heated test section (W)
$t_{v,P}$	Student-t value
T	temperature (K)
UI	estimated total uncertainty interval
$\dot{V}$	volumetric flow rate (m^3/s)
X_{tube}	total tube length (m)

Greek symbols

α	heat-transfer coefficient (W/m^2 K)
Γ	mass flow rate per unit length (kg/m s)
ΔT	temperature difference (K)
δ_c	reference film thickness (m)
ε	measurement accuracy
λ	thermal conductivity (W/m K)
μ	dynamic viscosity (N s/m^2)
ρ	density (kg/m^3)

Subscripts

core	central core in heat exchanger
f	fluid
flow	free flow in test section
g	gravity
he	heated area
l	liquid
m	measured
R	result
RSS	root sum square
shell	heat exchanger shell
tube	tube
v	vapor
w	wall

Abbreviations

C_1	methane
C_2	ethane
C_3	propane
nC_4	*n*butane
LNG	liquefied natural gas

for LNG heat exchangers. Three Ph.D. theses have been integrated as part of the research program [2–4].

The results from the measurements have been used to choose and develop calculation models for heat transfer and pressure drop. These models are implemented in different design and optimization tools for LNG plants [5], and in a user-added subroutine program for the process simulator PRO/II [6,7].

2. Experimental set-up

2.1. Description of test facility

A flow diagram of the test facility, including main equipment and instrumentation is shown in Fig. 2.

The facility consists of a test circuit, a propane brine circuit and a methane cooling circuit.

2.1.1. Test circuit

The test fluid is circulated through the test heat exchanger [A] as gas, liquid or two-phase flow. When measurements are performed at two-phase conditions, the fluid is separated into a liquid stream and a vapor stream in a drum [B] after the test exchanger. The flow rate is measured for the liquid [G] and vapor stream [D]. The vapor stream is circulated by a gas blower [C] and cooled [E] before it is mixed with the liquid stream at the test exchanger inlet. The liquid phase is circulated with a pump [F]. The gas and liquid flow is controlled by the use of frequency control on the blower and the pump motors. This provides a smooth regulation of the flow rates and vapor fraction through the test heat exchanger. The temperature of the propane brine controls the temperature in the test circuit. The pressure in the test circuit is controlled both by the temperature and by the total inventory.

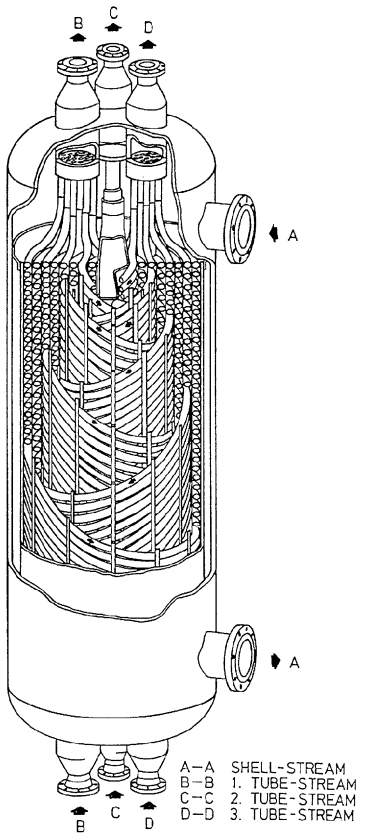

Fig. 1. Principal sketch of a multi-stream spiral-wound heat exchanger [1].

2.1.2. Propane brine circuit

The liquid and vapor streams in the test circuit are cooled by cold propane [E], [H]. The propane is circulated by a pump [I] and cooled in heat exchange with evaporating methane [K]. The brine circuit is branched into three courses; cooling of test fluid liquid phase, cooling of test fluid vapor phase and re-circulation of the brine. The propane flow rate is controlled by frequency regulation of the propane pump motor and the split ratio between the different courses. The brine temperature is controlled by regulation of the capacity of the cryogenerator [N] and by use of an electrical heater [J].

2.1.3. Methane cooling circuit

The main cooling circuit operates by use of thermosyphon circulation. The methane is condensed by the cryogenerator, which provides the refrigeration duty.

The operational ranges for the test facility are given in Table 1.

Table 1
Operational ranges for test facility

Parameter	Low range	High range
Temperature (°C)	−150	0
Pressure (bar)	1	15
Mass flux (kg/m^2 s)	20	200
Vapor fraction (kg/kg)	0	1
Heat flux (W/m^2)	0	10,000

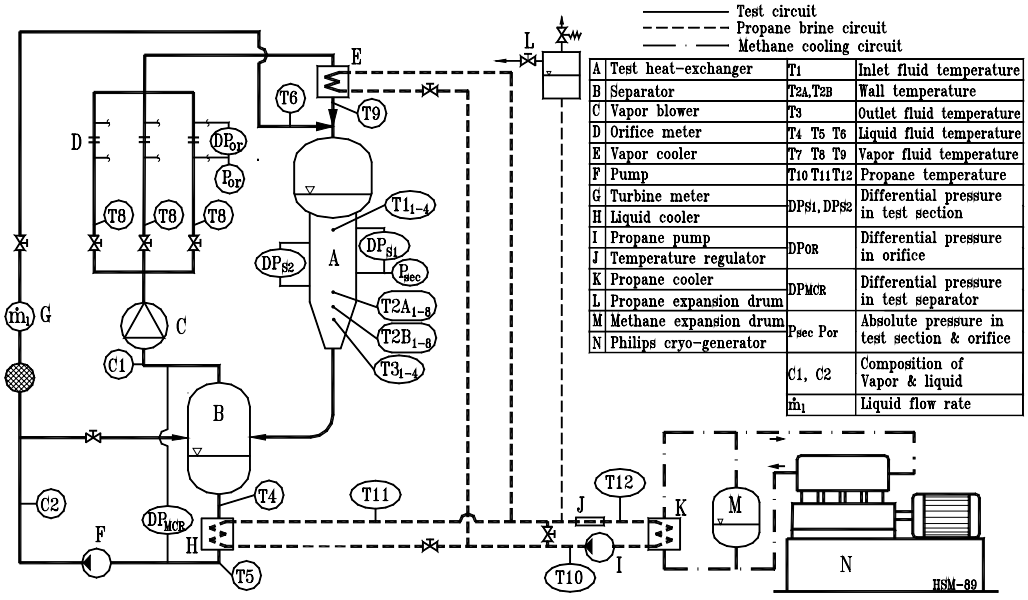

Fig. 2. Flow diagram of the test facility.

2.2. Test heat exchanger

A simplified sketch of the test heat exchanger is shown in Fig. 3.

The heat exchanger can be operated both in single-phase and two-phase flow. Before the distribution system the liquid and vapor flow is brought to thermodynamic equilibrium by a mixing system consisting of bends and T-junctions.

It is important to obtain uniform distribution of the two-phase flow in the test exchanger. The flow distribution system consists of a plate with 30 vertical tubes placed in a circle over the central coil. Each tube has two slits, 0.5 mm wide and 100 mm long. The two-phase flow is separated by gravity, and the liquid forms a level over the partition plate before it is drained through the slits in the tubes. The vapor is drained directly through the center of the tubes, and the two-phase flow forms an annular flow pattern through the distribution tubes. The expansion at the outlet of the tubes generates a uniform spray of liquid over the whole flow area in the test section.

The test section is a model of a spiral-wound heat exchanger, and consists of one central coil and two half-tube coils on the inner and outer walls. The center coil contains four parallel tubes and the inner and the outer coils consist of three and five parallel half-tubes, respectively. The half-tubes on the walls are inserted in order to obtain right flow performance around the center coil where the heat-transfer coefficient is measured. The main layer is coiled to the right and the two half layers are coiled to the left. Three longitudinal space bars are inserted between each of the layers. The tubes in the center coil are also separated by space bars in the longitudinal direction. The test section consists of a flow stabilization zone, an isothermal zone and an electrically heated zone. The tubes in the central coil are electrically heated by heating cables placed inside the tubes. Pressure drops are measured in the isothermal zone and heat-transfer coefficients are measured in the heated zone. The heated zone is separated from the rest of the heat exchanger by Teflon plugs in order to prevent heat leakage.

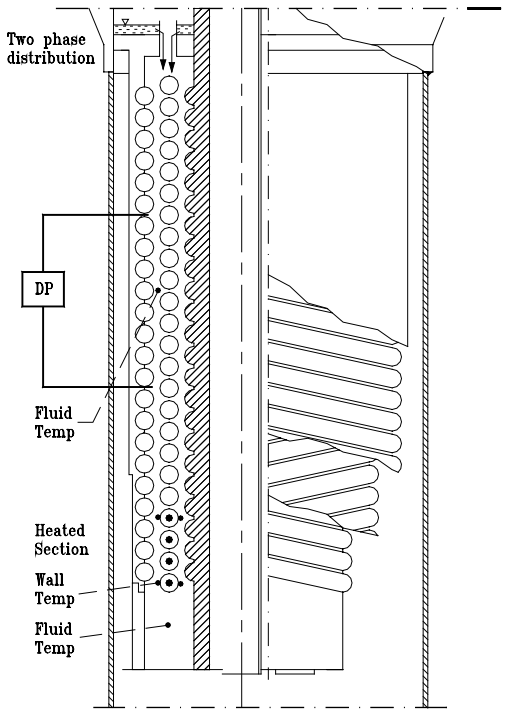

Fig. 3. Test heat exchanger.

2.2.1. Flow area in test section

For calculation of flow velocity in the test section the free flow area has to be calculated. In general the flow area is calculated from Eq. (1) [2]:

$$A_{\text{flow}} = \pi \cdot \left[\frac{D_{\text{core}} + D_{\text{shell}}}{2} \right] \cdot N_{\text{lay}} \cdot S_{\text{ref}} \tag{1}$$

S_{ref} is the radial distance between two neighboring tubes and different methods for the calculation exist. The tube configuration varies continuously between in-line and staggered. The in-line configuration gives a minimum radial distance, while the staggered gives the maximum. In the derivation and development of calculation methods for heat-transfer coefficients and frictional pressure drops the in-line flow area is applied (Eq. (2)):

$$S_{\text{ref}} = S_{\text{in}} = P_r - D_{\text{tube}} \tag{2}$$

The geometrical data for the test section are given in Table 2.

Table 2
Geometrical data of the test exchanger

Parameter	Value
Outside tube diameter	12.00 ± 0.05 mm
Longitudinal distance between tube centers	13.94 ± 0.09 mm
Radial distance between tub centers	15.91 ± 0.06 mm
Winding angle	$7.938 \pm 0.06°$
Core diameter (between top of half-tubes)	108.0 ± 0.05 mm
Shell diameter (between top of half-tubes)	147.63 ± 0.2 mm
Height of test exchanger	336 mm
Vertical distance between pressure taps	126 mm
Height of heated zone	56 mm
Heated tube length	1688.5 ± 3.00 mm
Heated area	$63{,}655.0 \pm 288$ mm^2
In-line flow area	3031.2 ± 63 mm^2

2.3. Instrumentation and accuracy

In order to calculate local heat-transfer coefficients and pressure drops, measurements of different parameters have to be done. During operation of the plant some data are taken for control purposes, adjustment and stabilization. The main categories of measurements are: temperature, absolute pressures, differential pressures, flow rates, heat flux and fluid composition. In Fig. 2 the main instrumentation is shown. An automatic logging system samples data from the different instruments. A Keithley 2001 multi-meter and a Keithley 7001, 80 channel scanner are applied. The raw data are collected in a PC and further processed by a separate data analysis routine.

The accuracy of measured data as well as thermophysical properties are used to estimate the total measurement accuracy of derived data such as flow rates, vapor fraction, local frictional pressure drop and local heat-transfer coefficients.

2.4. Treatment of errors

Measured and derived parameters are combined by functional relationships into the result. The estimated errors for each parameter must therefore also be propagated into the results. A result, R, is derived from J number of variables with different average values, x_j (Eq. (3)):

$$R = R\langle x_1, x_2, \ldots, x_j, \ldots, x_J\rangle \pm \mathrm{UI} \tag{3}$$

Each x_j may contain both systematic and random errors. The aim is to estimate a total uncertainty interval for the result, and the variables should, as far as possible, be independent of each other.

For the combination of errors the root sum squares approach is well known and frequently applied (Eq. (4))

$$\mathrm{UI}_{\mathrm{R,RSS}} = \sqrt{B_{\mathrm{R}}^2 + (t_{v,\mathrm{P}} \cdot S_{\mathrm{R}})^2} \tag{4}$$

B_{R} is the estimated total error from systematic error sources and S_{R} is the total standard deviation from random errors. For the Student-t value, $t_{v,\mathrm{P}}$, a 95% probability is used.

A more thorough description of the treatment and propagation of errors are described by Fredheim [2].

2.5. Thermodynamic and physical properties

The in-house software TP-lib [7] is used for the calculation of thermodynamic and physical properties. The Peng Robinson equation of state (PR-EOS) [8,9] is used for thermodynamic calculations.

The density is calculated using a corresponding state method as described by Ely and Hanley [10] and Stephan and Heckenberger [11]. Viscosity and thermal conductivity are calculated by a corresponding state method similar to the method used for calculation of density. A review of this method can be found from Ely and Hanley [10]. The corresponding state methods were selected because they can handle both pure components and mixtures. The method uses methane as reference fluid.

The accuracy of the used methods is given in Table 3.

Table 3
Relative accuracy of thermophysical properties

Property	Accuracy (%)
Specific heat capacity	5
Density	2
Thermal conductivity	8
Viscosity	8

3. Data reduction

The heat-transfer coefficient in the test section is calculated by Eq. (5):

$$\alpha = \frac{Q_{\mathrm{sec}}}{A_{\mathrm{he}} \cdot \Delta T} = \frac{Q_{\mathrm{sec}}}{A_{\mathrm{he}} \cdot (T_{\mathrm{w}} - T_{\mathrm{f}})} \tag{5}$$

Q_{sec} is the electrical power supplied to the heated zone of the test exchanger. T_{w} is the average wall temperature in the upper part of the heated zone. T_{f} is the fluid temperature at the same position as the upper wall-temperature measurements. T_{f} is calculated from the measured average fluid temperatures at the inlet and outlet of the heated zone, assuming a linear longitudinal temperature profile between inlet and outlet.

The total flow rate is calculated from Eq. (6):

$$\dot{m}_{\mathrm{tot}} = \dot{m}_{\mathrm{v}} + \dot{m}_{\mathrm{l}} = \dot{m}_{\mathrm{v}} + \dot{V}_{\mathrm{l}} \cdot \rho_{\mathrm{l}} \tag{6}$$

The vapor flow rate is calculated directly from the orifice meter based on the measured pressure drop and temperature [12].

The liquid flow rate is calculated from the measured volumetric flow from the turbine meter and the liquid density in the turbine meter.

The uncertainty in total fluid flow rate is calculated during the data reduction.

4. Experimental results

The experimental results from measurements of liquid falling film flow are presented. The range of the measurements by means of test fluid and operational conditions is described in Table 4. A total of 171 test runs have been accomplished.

Table 4
Operational conditions

Fluid	Temperature (°C)	Pressure (bar)	Flow (kg/m^2 s)	Re_l (–)	Pr_l (–)	n (–)
C_3 (1991)	−30 to −5	1.6–4.0	27–120	1400–5600	2.80–2.95	35
C_3 (1999)	−25 to −5	2.0–4.0	7–113	500–5800	2.80–2.92	58
C_2	−75 to −47	2.0–6.2	27–119	1500–8000	2.26–2.37	27
C_2/C_3 10/90 mol%	−30 to −15	2.2–3.6	35–98	1900–5000	2.86–2.94	14
C_2/C_3 15/85 mol%	−19 to −17	3.6–3.8	36–89	1800–4700	2.83–2.84	7
C_2/C_4 30/70 mol%	−37 to −5	2.0–4.0	45–85	1400–2600	3.48–3.77	10
C_1/C_2 41/59 mol%	−134 to −105	2.0–4.0	15–96	700–5600	2.15–2.56	20

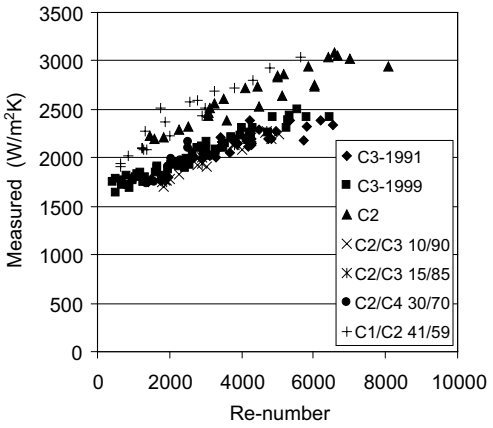

Fig. 4. Measured heat-transfer coefficients (α).

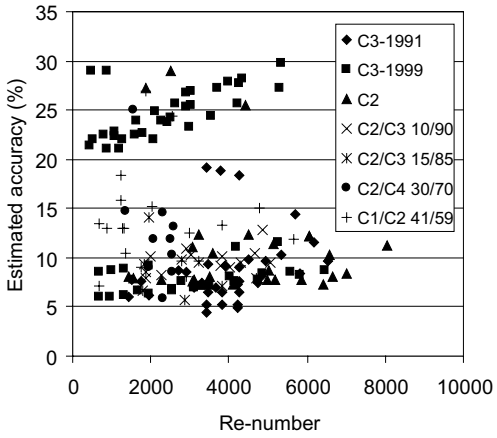

Fig. 5. Estimated measurement accuracy for heat-transfer coefficients.

All measured heat-transfer coefficients are shown in Fig. 4 and the corresponding estimated measurement accuracy is given in Fig. 5. Some of the data have quite poor measurement accuracies. This is mainly due to low temperature difference between the test fluid and the heated wall.

For the measurements with methane/ethane mixture as test fluid, selected measured and calculated data are tabled in Table 5.

The *Nu*-number for the liquid film, Nu_l is calculated from Eqs. (10) and (11). The *Re*-number for the liquid film, Re_l, is calculated from Eq. (13). The *Pr*-number for the liquid film, Pr_l, is calculated from Eq. (14).

5. Calculation model

For calculation of heat-transfer coefficients for gravity dominated liquid falling film flow a method from Bays and McAdams [13] is used, Eq. (7).

$$\alpha = a \cdot \left[\frac{2 \cdot \lambda^2 \cdot \rho^{4/3} \cdot g^{2/3} \cdot c_p}{\pi \cdot D_{\text{tube}} \cdot \mu^{1/3}}\right]^{1/3} \cdot \left[\frac{4 \cdot \Gamma}{\mu}\right]^b \tag{7}$$

Γ is the mass flow rate per unit length (Eq. (8)):

Table 5
Data for heat-transfer measurements with methane/ethane mixture

P (bar)	T (°C)	M (kg/m^2 s)	Re_l (–)	Pr_l (–)	Nu_l (–)	α_m (W/m^2 K)	ε_α (%)
2.049	−133.29	17.67	658	2.55	0.240	1938.6	7.19
2.035	−133.63	34.54	1280	2.55	0.258	2077.2	13.02
2.034	−133.68	46.93	1738	2.55	0.312	2516.1	8.98
2.040	−133.61	74.77	2774	2.55	0.322	2595.3	9.68
2.050	−133.48	86.97	3235	2.55	0.334	2691.5	9.62
4.070	−104.56	14.58	864	2.15	0.240	2014.4	12.97
4.032	−105.25	23.36	1371	2.16	0.249	2084.3	10.52
4.036	−105.12	49.51	2913	2.16	0.290	2428.2	8.15
4.033	−105.06	73.08	4305	2.15	0.333	2794.8	9.25
4.029	−105.10	95.83	5645	2.16	0.362	3036.5	11.93

$$\Gamma = \frac{\dot{m}_l}{2 \cdot X_{tube}} \tag{8}$$

X_{tube} is the total tube length, perpendicular to the flow direction (Eq. (9)):

$$X_{tube} = \pi \cdot \left[\frac{D_{core} + D_{shell}}{2} \right] \cdot N_{lay} \tag{9}$$

Eq. (7) may also be written in a dimensionless form as given in Eqs. (10)–(14).

$$Nu_l = a_1 \cdot \left(\frac{D_{tube}}{\delta_c} \right)^c \cdot Re_l^b \cdot Pr_l^d \tag{10}$$

$$Nu_l = \frac{\alpha \cdot \delta_c}{\lambda} \tag{11}$$

$$\delta_c = \left[\frac{\mu^2}{g \cdot \rho^2} \right]^{1/3} \tag{12}$$

$$Re_l = \frac{4 \cdot \Gamma}{\mu} \tag{13}$$

$$Pr_l = \frac{\mu \cdot c_p}{\lambda} \tag{14}$$

For $Re_l \leqslant 2000$ constants from Bennett et al. [14] are used. For $Re_l > 2000$ new constants are fitted.

$Re_l \leqslant 2000$

$a = 0.886, \quad a_1 = 0.762, \quad b = 1/9, \quad c = -1/3, \quad d = 1/3$

$Re_l > 2000$

$a = 0.313, \quad a_1 = 0.269, \quad b = 1/4, \quad c = -1/3, \quad d = 1/3$

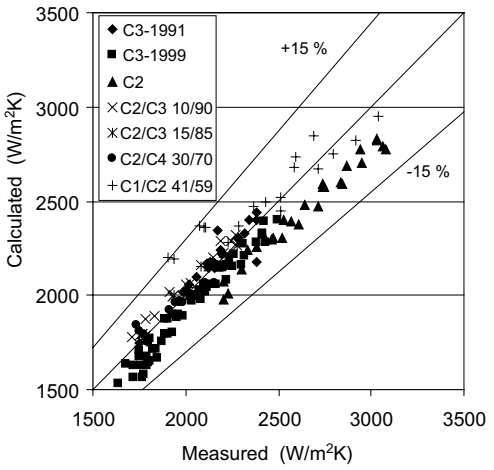

Fig. 6. Measured and calculated heat-transfer coefficients.

Table 6
Deviation between calculated and measured heat-transfer coefficients

Test fluid (mol%)	Mean deviation (%)	Abs. mean deviation (%)	Standard deviation (%)
C_3 (1991)	0.59	1.73	2.45
C_3 (1999)	−4.66	4.66	2.96
C_2	−7.11	7.11	1.68
C_2/C_3 10/90	3.11	3.11	1.43
C_2/C_3 15/85	1.27	1.51	1.36
C_2/nC_4 30/70	0.28	1.90	2.81
C_1/C_2 41/59	4.42	5.60	6.03

A comparison between the measured values and the calculated by the use of the method from Bays and McAdams is given in Fig. 6.

As the figure shows, the agreement between the calculated and measured data is good and better than ±15% for all data points. Most of the data are within ±10%.

A summary of the agreement between the selected calculation model for heat-transfer coefficients and the measured values is given in Table 6.

6. Conclusions

Measurements of local heat-transfer coefficients for liquid falling film flow on the shell-side of a spiral-wound LNG heat exchanger have been worked out. Based on the measurements, using various pure and mixed hydrocarbons as test fluids, a known method for calculation of heat-transfer coefficients is tested and further improved. Calculated values are compared to the measured ones. The agreement between calculated and measured values is mainly good. For calculation of heat-transfer coefficients a method from Bays and McAdams [13] is recommended. The average deviation is within ±7% compared with the measured values. The measurement accuracy varies between ±5–30%.

Acknowledgements

The work is mainly financed by Statoil Research Center. The technical staff of SINTEF Energy Research and NTNU has done a good effort in the construction, as well as for support during the time of operation, of the test plant.

References

[1] A.G. Linde, Catalogue entitled Rohrbündel-Wärmeaustaucher, Linde A.G. Werksgruppe, TVT, Munich, Germany.
[2] A.O. Fredheim, Thermal design of coil-wound LNG heat exchangers, shell-side heat transfer and pressure

drop, Ph.D. Thesis, Norwegian Institute of Technology, 1994.
[3] B. Aunan, Shell-side heat transfer and pressure drop in coil-wound LNG heat exchangers, laboratory measurements and modeling, Ph.D. Thesis, The Norwegian University of Science and Technology, 2000.
[4] B.O. Neeraas, Condensation of Hydrocarbon Mixtures in Coil-wound LNG Heat Exchangers, Tube-side Heat Transfer and Pressure Drop, Norwegian Institute of Technology, 1993.
[5] G. Owren et al., The LNG plant design optimization tool CryoPro, a joint venture, in: Proceedings of AIChE Spring National Meeting, New Orleans, 1992.
[6] A.O. Fredheim et al., Coil, a model for simulation of spiral wound LNG heat exchangers, in: Proceedings from World Gas Conference 2000, Nice, June 2000.
[7] PRO/II. Steady-state flowsheeting and process optimisation software, Simulation Sciences Inc.
[8] R.O. Peng, D.B. Robinson, A new two-constant equation of state, Ind. Eng. Chem. Fundament. 15 (1) (1976) 59–64.
[9] J.M. Prausnitz et al., Molecular Thermodynamics of Fluid-Phase Equilibria, second ed., PTR Prentice-Hall, ISMN:0-13-599564-7, 1986.
[10] J.F. Ely, H.J.M. Hanley, A computer program for the prediction of viscosity and thermal conductivity in hydrocarbon mixtures, National Bureau of Standards, NBS Technical note1039, 1981.
[11] K. Stephan, T. Heckenberger, Thermal conductivity and viscosity data of fluid mixtures, DECHEMA Chemistry data Series, vol. 10, Part 1, 1987.
[12] DIN 1952, Measurement of fluid flow by means of orifice plates, nozzles and venturi tubes inserted in circular cross-section conduits running full, VDI-rules for measurement of fluid, 1980.
[13] G.S. Bays, W.H. McAdams, Heat transfer coefficients in falling film heaters, streamline flow, Indust. Eng. Chem. 29 (11) (1937) 1240–1246.
[14] D.L. Bennet, B.L. Hertzler, C.E. Kalb, Down-flow shell-side forced convective boiling, AIChE J. 32 (12) (1986) 1963–1970.